Journal of Power Sources 232 (2013) 323–331

Contents lists available at SciVerse ScienceDirect

Journal of Power Sources

journal homepage: www.elsevier.com/locate/jpowsour

Ab initio design of GaN-based photocatalyst: ZnO-codoped GaN nanotubes

Yao Kun Lim [a], Eugene Wai Keong Koh [a], Yong-Wei Zhang [b], Hui Pan [b,*]

[a] Department of Materials Science and Engineering, National University of Singapore, 9 Engineering Drive 1, Singapore 117576, Singapore
[b] Institute of High Performance Computing, A*STAR, Singapore 138632, Singapore

HIGHLIGHTS

- GaN nanotubes codoped with ZnO.
- Chirality-dependent doping effects.
- Wide tunable band gap and enhanced mobility.
- High efficiency for solar energy conversion.

GRAPHICAL ABSTRACT

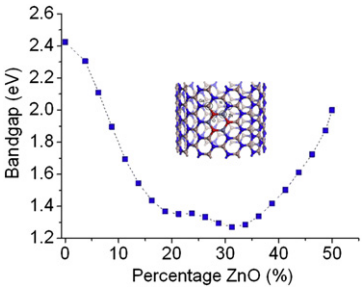

ARTICLE INFO

Article history:
Received 3 December 2012
Received in revised form
9 January 2013
Accepted 13 January 2013
Available online 19 January 2013

Keywords:
Gallium nitride nanotube
Zinc oxide codoping
Band gap engineering
Photocatalyst
Hydrogen generation
First-principles calculation

ABSTRACT

ZnO-codoped GaN nanotubes are designed and studied for their application as photocatalyst on the basis of first-principles calculations. The codoped nanotubes are semiconducting with their band structures controllable by the doping concentration. It is found that the codoping and its effects on the band gaps strongly depend on the chirality of the nanotubes. For armchair nanotubes, the ZnO codoping prefers to the radial direction of the nanotube, and a minimum of band gap at 1.27 eV is achievable at the concentration of 31 at.%. For zigzag nanotubes, the codoping is energetically more stable in the axial direction, and a reduction of 21% in band gap can be obtained by optimizing the doping concentration. The calculated potentials of the conduction band bottoms of the codoped nanotubes are more negative than H_2/H_2O level, and those of their valence band tops are more positive than O_2/H_2O level. The calculated electronic properties of the codoped nanotubes evidence the widely tunable band gap, enhanced mobility, and better band edges' alignments, satisfying basic prerequisites as a new class of high efficiency photocatalysts for water splitting and other avenues of solar energy utilization.

1. Introduction

The demand for energy is projected to more than double by 2050 and to more than triple by the end of the century. Incremental improvements in existing energy networks will not be adequate to supply this demand in a sustainable way. Finding sufficient supplies of clean energy for the future is one of society's most daunting challenges due to the limited supply of the old forms of depletable energy (coal, oil, nuclear) and their detrimental effects on the global climate. Solar energy is considered to be the most important candidate because it is abundant, clean and renewable. A variety of technologies have been developed to take advantage of solar energy, such as solar electricity (photovoltaic cell–PV), solar fuels (photo-electrochemical cell–PEC), and solar thermal systems. The PEC, which splits water into hydrogen and oxygen, so as to convert the solar energy into chemical energy, has attracted increasing

* Corresponding author. Tel.: +65 64191425; fax: +65 64674350.
E-mail address: panh@ihpc.a-star.edu.sg (H. Pan).

0378-7753/$ – see front matter © 2013 Elsevier B.V. All rights reserved.
http://dx.doi.org/10.1016/j.jpowsour.2013.01.066

attention since the discovery of water splitting property of TiO_2 electrodes under ultraviolet (UV) illumination [1] due to the versatile applications of hydrogen and oxygen gases. However, the UV irradiation only accounts for ~5% of the solar spectrum and, as a consequence, the solar energy conversion efficiency of TiO_2 is limited due to its wide band gap (~3.0 eV). To enhance the efficiency, considerable efforts have been conducted to fine tune its band gap for the visible-light absorption, such as chemical functionalization, surface-decoration, coating, doping, and defect-engineering [2–19], but only limited success has been achieved to date. Design of new photocatalysts is thus a critical step to solar energy harvesting. The development of efficient photocatalysts should satisfy: (1) an optimal band structure for maximal utilization of solar energy [2,7,20,21], (2) efficient photo-induced electron–hole separation and high carrier mobility [22], (3) large contacting surface area with the electrolyte [3], and (4) high stability in extreme environments [23]. Based on these principles, many new photocatalysts using transition-metal oxides as the main component have been proposed and tested [24]. However, the low carrier mobility and high recombination rate in transition-metal oxides induced by the localized *d* states at the band edge limit the conversion efficiency. It was proposed that the delocalized s/p states (at the band edges) of the materials, such as metal-free compound (graphitic carbon nitride) [25,26], may shed light on the enhancement of carrier mobility. Recently, it was reported that the gallium nitride/zinc oxide alloy (GaN/ZnO) with its band edges' states dominated by the s/p states showed excellent performance for the H_2 and O_2 production from water under visible-light irradiation [27–31]. The alloy can be easily produced by the thermal-treatment of Ga/Zn oxide under ammonia at high temperature [27]. On the other hand, the nanostructures of these materials show promising potency to enhance the solar energy harvesting by improving light trapping, photo-carrier collection, and contacting surface area [32]. In the present study, GaN nanotubes codoped with Zn and O are designed for possible applications in solar energy conversion based on first-principles calculation. It is shown that the conversion efficiency of the codoped GaN nanotubes is improved due to the narrowing of band gap, enhancement of visible-light absorption, suitable band edges' alignment vs. hydrogen normal electrode, and improvement of mobility, compared with the counterparts without doping.

2. Methods

The first-principles calculation was carried out based on the density functional theory [33] and the generalized gradient approximation (GGA) [34] as incorporated in the Vienna *ab initio* simulation package (VASP) [35]. The Monkhorst and Pack scheme of *k* point sampling was used for integration over the first Brillouin zone [36]. The Hubbard on-site Coulomb interaction parameter U–J (=2 eV) for Ga was chosen to make the lattice constants of bulk GaN comparable with the experimental values. The U–J for Zn was 6 eV for the codoping of ZnO. A $1 \times 1 \times 7$ grid for k-point sampling and an energy cutoff of 450 eV were consistently used in our calculations on GaN nanotubes. Good convergence was obtained using these parameters, and the total energy was converged to 2.0×10^{-5} eV/atom. A large supercell dimension with a wall–wall distance of 10 Å in the plane perpendicular to the tube axis was used to avoid interaction between the nanotube and its images in neighboring cells. Two nanotubes with different chirality, that is, armchair GaN (10, 10) (GaN-ac10) and zigzag GaN (12, 0) (GaN-zz12) [37], were studied. The periodic units in the axial direction are 12.33 and 16.5 Å for armchair and zigzag nanotubes, respectively.

The engineering of the electronic structure of the GaN nanotube for its application in solar energy conversion is realized by doping the nanotube with Zn, O, and both of them (Fig. 1). The formation energy of substitution is estimated from

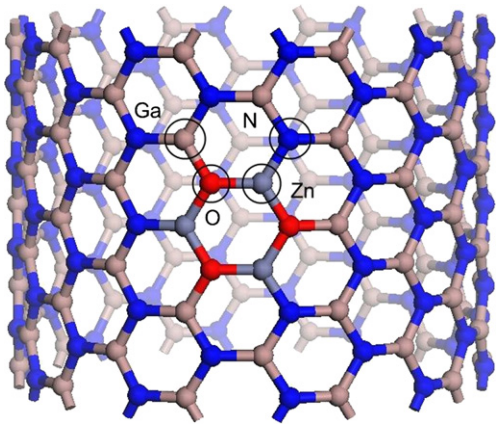

Fig. 1. Atomic configurations of an armchair GaN nanotube (10, 10) codoped with ZnO. Different atoms are represented by different colors: O: red, Zn: gray, N: blue, and Ga: brown). (For interpretation of the references to color in this figure legend, the reader is referred to the web version of this article.)

$$E_f = E_{\mathrm{tot}}(\mathrm{tube}+\mathrm{doping}) - E_{\mathrm{tot}}(\mathrm{tube}) - n\mu_{\mathrm{O}} - m\mu_{\mathrm{Zn}} + n\mu_{\mathrm{N}} + m\mu_{\mathrm{Ga}} \quad (1)$$

where E_{tot}(tube + doping) and E_{tot}(tube) are the total energies of the GaN nanotubes with and without doping, respectively; μ_{Zn} and μ_{Ga} are the chemical potentials (the energy required to remove an atom from its bulk) of the metal elements, *m* is the number of the metal atoms, and *n* is the number of oxygen/nitrogen atoms [38]. $\mu_{\mathrm{O}} = 1/2E(O_2)$ and $\mu_{\mathrm{N}} = 1/2E(N_2)$, where $E(O_2)$ and $E(N_2)$ are the energy of the oxygen and nitrogen molecule.

3. Results and discussion

The geometries of the GaN nanotubes are fully relaxed before we study the doping effects. The calculated Ga–N bond length in the nanotube is ~1.83 Å, which is less than that in bulk, and consistent with literature [37]. The stability and possibility of the doping are investigated by calculating the formation energy (E_f) of substitution (Eq. (1)). The calculated energies are about −1.9 and 4.3 eV for O and Zn substitutions of N and Ga, respectively, indicating that O-doping is much easy, while Zn-doping is difficult (Table 1) because oxygen is easier to attract electrons than nitrogen to form Ga–O bond, while Zn is more difficult to give out electrons than Ga to form Zn–N bond. To improve Zn-doping, we study the ZnO codoping. The energies of the codoping in GaN-ac10 and GaN-zz12 are about −0.43 and −0.51 eV, respectively. Although the energies of codoping are higher than the O-doping energy, they are much lower than the Zn-doping energy, confirming that the codoping can improve the possibility of Zn substitution in GaN nanotubes due to the electrostatic attraction between the two atoms (Zn and O) with opposite charges [39]. The more negative charged O (compared with N) can attract less positive charged Zn by forming ZnO bond in the nanotube, leading to the easy

Table 1
The formation energies of substitutions of N, Ga, and GaN pair with O, Zn and ZnO pair, respectively.

	O_N (eV)	Zn_{Ga} (eV)	ZnO_{GaN} (eV)
GaN-ac10	−1.88	4.28	−0.43
GaN-zz12	−1.97	4.28	−0.51

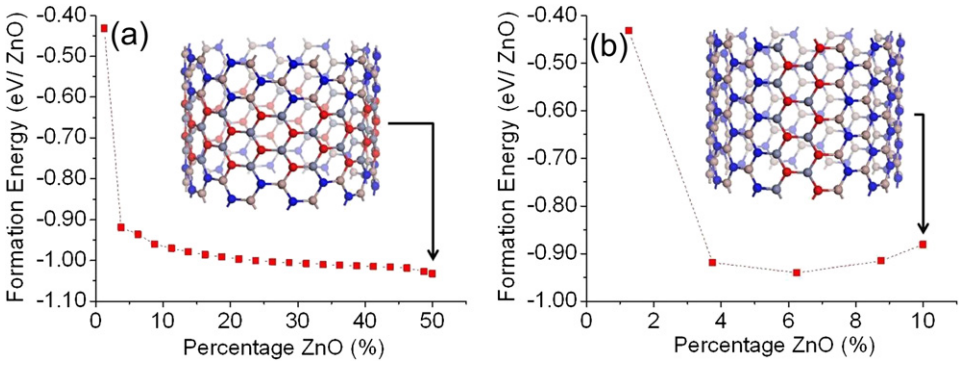

Fig. 2. Formation energy of ZnO codoping in armchair nanotube (10, 10) as a function of doping concentration: (a) ZnO-codoping in the radial direction. The inset shows the structure with ZnO doped at a concentration of 50 at.%. (b) ZnO-codoping in the axial (z) direction. The inset shows the structure with ZnO doped at a concentration of 10 at.%.

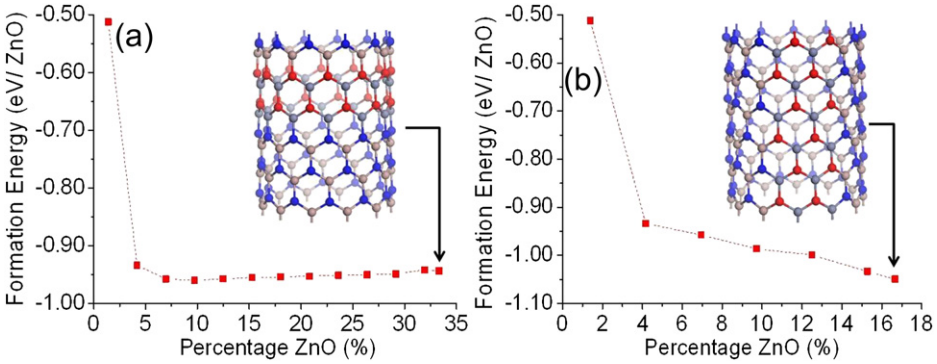

Fig. 3. Formation energy of ZnO codoping in zigzag nanotube (12, 0) as a function of doping concentration: (a) ZnO-codoping in the radial direction. The inset shows the structure with ZnO doped at a concentration of 33 at.%. (b) ZnO-codoping oriented in the z direction. The inset shows the structure with ZnO codoped at a concentration of 17 at.%.

incorporation of the pair into the host material. We further investigate the formation energy of the codoping as a function of the doping concentration. For GaN-ac10, the formation energy decreases sharply when a GaN hexagon in the GaN nanotube is substituted by a ZnO hexagon (three ZnO pairs) (Fig. 2), indicating that the 3-pair ZnO codoping in hexagon is more stable than 1-pair ZnO. The 3-pair ZnO codoping in hexagon is also more stable than 3-pair ZnO random codoping, with the former having a formation energy of −0.92 eV/pair, and the latter −0.49/pair. Hence, instead of random codoping, hexagonal codoping of ZnO is considered. Increasing the ZnO concentration further, the formation energy decreases slowly if the codoping is along the radial direction (inset in Fig. 2(a)) (Fig. 2(a)), while it slightly increases if the codoping is along the axial (or z) direction (inset in Fig. 2(b)) (Fig. 2(b)). Importantly, we see that the formation energy of the codoping along the radial direction is lower than that along the z direction, indicating that the codoping in the radial direction of armchair nanotube is easy and a hetero-superlattice GaN/ZnO nanotube is

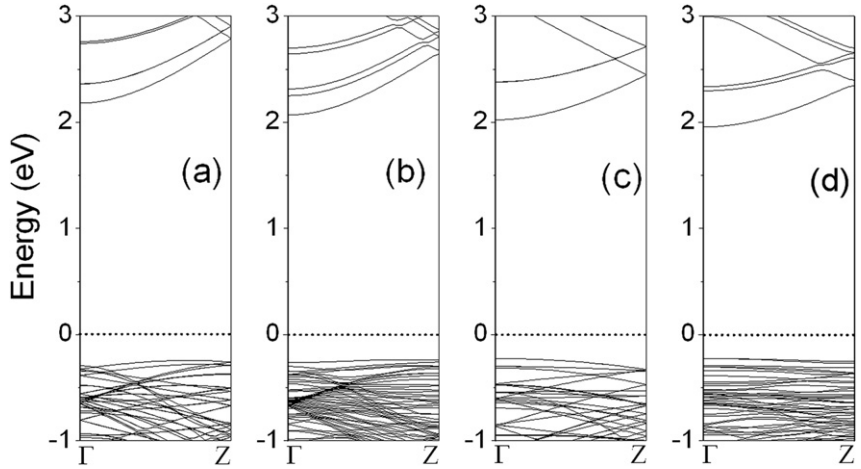

Fig. 4. The calculated band structures. (a) Pristine GaN-ac10, (b) GaN-ac10 doped with a ZnO hexagon, (c) pristine GaN-zz12, and (d) GaN-zz12 doped with a ZnO hexagon. The Fermi level is shifted to 0 eV (dotted line).

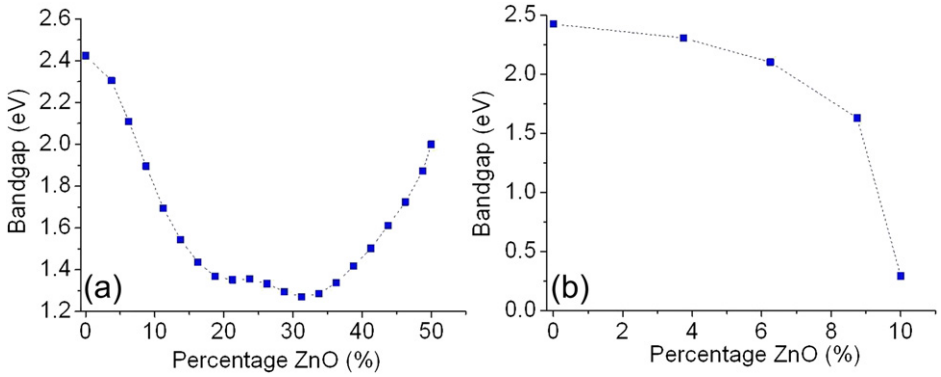

Fig. 5. The calculated band gap of armchair (10, 10) nanotube as a function of ZnO concentration: (a) ZnO oriented in the radial direction, and (b) ZnO oriented in the *z* direction.

possible. Similarly for GaN-zz12, the formation energy initially decreases sharply when a GaN hexagon in GaN nanotube is substituted by a ZnO hexagon (Fig. 3). The hexagon ZnO codoping ($E_f = -0.93$ eV/pair) is also more stable than 3-pair ZnO random codoping ($E_f = -0.55$ eV/pair). The formation energy of the codoping increases slowly with the increase of the ZnO concentration along the radial direction (Fig. 3(a)), while it decreases if the codoping is along the *z* direction (Fig. 3(b)). For the zigzag nanotube, the codoping in the *z* direction is easier than that in the radial direction because of the relatively lower formation energy (Fig. 3). From the calculated formation energy, we see that the codoping is chirality-dependent, and is easier if the ZnO/GaN interface in the nanotube is armchair (insets in Fig. 2(a) and Fig. 3(b)), compared with the zigzag interface (insets in Fig. 2(b) and Fig. 3(a)).

The electronic structures of the pristine and doped GaN nanotubes are shown in Fig. 4. The pristine GaN-ac10 is an indirect semiconductor with conduction band bottom (CBB) at Γ point and valence band top (VBT) at 2/3 in the ΓZ direction (Fig. 4(a)), while GaN-zz12 is a direct semiconductor with both of CBB and VBT at Γ point (Fig. 4(c)). The band gaps are 2.42 and 2.25 eV for armchair and zigzag tubes respectively. Their band structures are affected by the codoping, as shown in Fig. 4(b) and (d). The codoped GaN-ac10 is still an indirect semiconductor with a narrowed band gap (Fig. 4(b)). Its CBB at Γ point shifts down and VBT shifts to Z point and slightly goes up. The codoped GaN-zz12 is still a direct semiconductor with CBB and VBT shifting closer at Γ point (Fig. 4(d)). From the calculated electronic structures, we see that the band gaps of GaN nanotubes are narrowed by ZnO-codoping at a low concentration. To efficiently control their band structures for optimal sunlight absorption, we further study the effect of the concentration of ZnO-codoping on the band gap.

The calculated band gaps of the codoped armchair GaN nanotubes at various ZnO concentrations are shown in Fig. 5. When the codoping is along the radial direction (inset in Fig. 2(a)), we see that

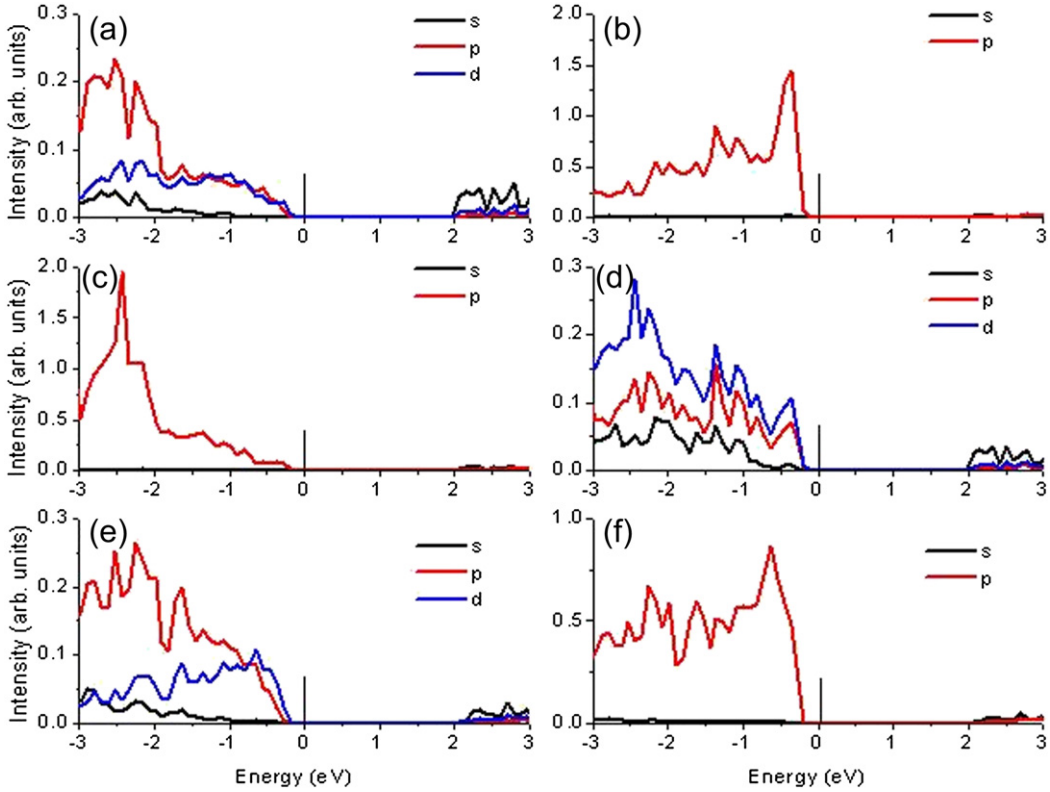

Fig. 6. The calculated partial density of states (PDOSs) of ZnO-codoped armchair GaN nanotube with concentration at 3.75 at.% (one hexagon ZnO): (a) Ga, (b) N, (c) O, (d) Zn interface atoms, (e) Ga and (f) N bulk atoms. The Fermi level is at 0 eV.

the band gap decreases sharply to 1.37 eV with the concentration of ZnO in the nanotube increasing up to 19 at.%, and then slowly to 1.27 eV by increasing the concentration to 31 at.%, but then increases relatively quickly to 2.0 eV with further increasing the concentration to 50 at.% (Fig. 5(a)). If the codoping is along the *z* direction (inset in Fig. 2(b)), the band gap decreases slowly with the increase of the concentration, and then goes down sharply to 0.29 eV when the ZnO hexagons are extended continuously along the *z* direction of the nanotube (Fig. 5(b)). The calculated PDOSs of the GaN-ac10 codoped with ZnO in radial direction reveal the origin of the change of the band gap (Fig. 6–8). The analysis on the partial density of state (PDOSs) of the ZnO-codoped GaN-ac10 with concentration at 3.75 at.% shows that the VBT is dominated by the p electrons of N atoms (Fig. 6(b)) and partially attributed to p electrons of O atoms (Fig. 6(c)) at the interface. The s states from Ga and Zn at the interface mainly contribute to the CBB states (Fig. 6(a) and 6(d)). The Ga and N atoms in the bulk (not at the interface) have no contribution to the band edge states (Fig. 6(e) and (f)). For the GaN-ac10 with a ZnO concentration of 31 at.%, the VBT is dominated by p electrons of N atoms (Fig. 7(d)) and partially has contribution from Ga atoms in the bulk (Fig. 7(c)). The p electrons of Ga and N atoms near to the doping site (Fig. 7(a) and (b)), s and p electrons of O atoms, and d electrons of Zn atoms (Fig. 7(e)–(h)) has little contribution to the VBT and lies deeper within the VB. The CBB is attributed to s states of Ga (interface) (Fig. 7(a)), O (interface and bulk) (Fig. 7(e) and (g)), and Zn (interface and bulk) (Fig. 7(f) and (h)). The band gap of the nanotube is at the minimum of 1.27 eV due to strong type-II band alignment. However, for the GaN-ac10 with a ZnO concentration of 50 at.%, the p electrons of N atoms at the interface dominate the VBT (Fig. 8(b)). The p electrons of N atoms in the bulk (Fig. 8(d)) and d electrons from Ga (Fig. 8(a) & (c)), and Zn atoms (interfacial and bulk) (Fig. 8(f) & (h)) also partially contribute the VBT, resulting in increase of band gap due to weak type-II band alignment. For its CBB, the contributions are from s states of Ga (interface) (Fig. 8(a)), O (interface and bulk) (Fig. 8(e) and (g)), and Zn (interface and bulk) (Fig. 8(f) and (h)). We clearly see that the origin of the VBT determines the band gap because the CBB almost has the same origin in the codoped nanotubes. The VBT is

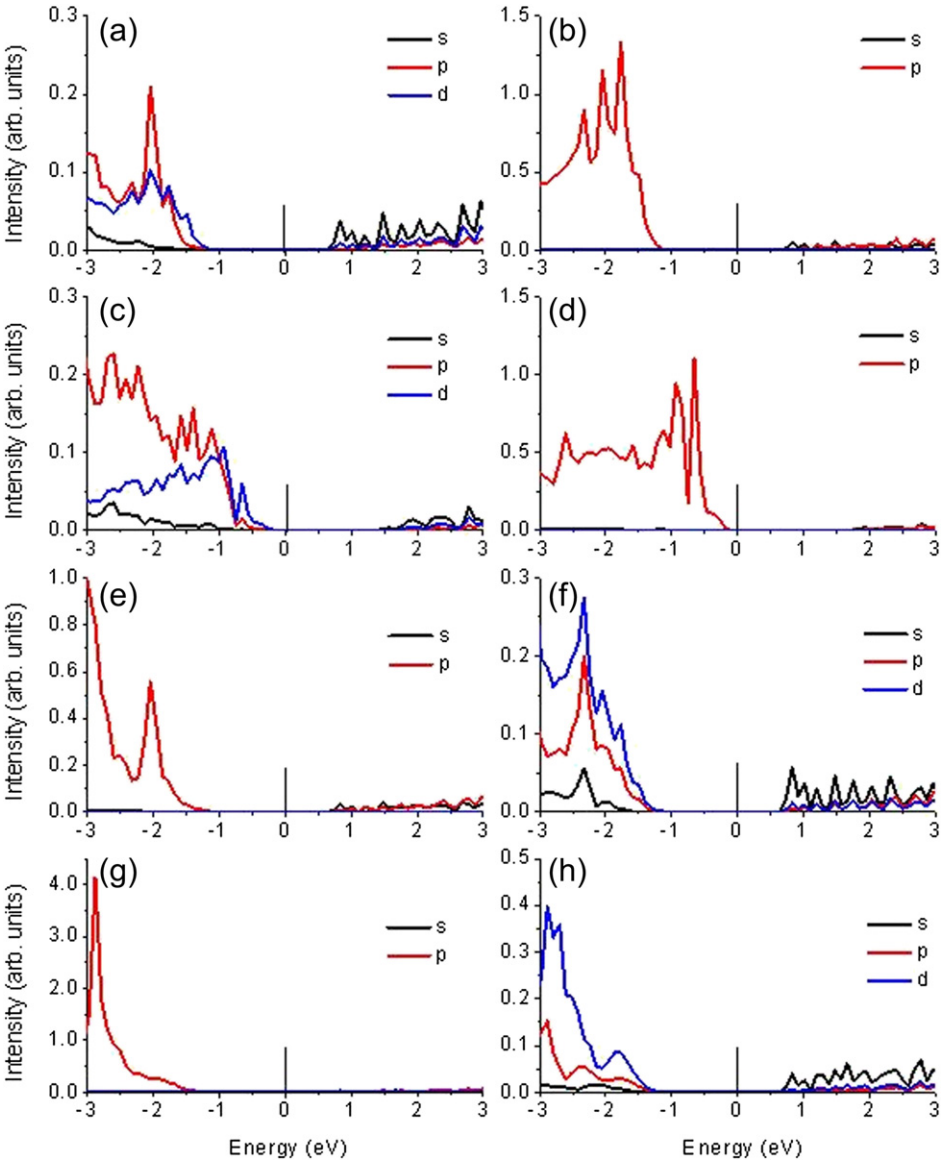

Fig. 7. The calculated partial density of states (PDOSs) of ZnO-codoped armchair GaN nanotube with concentration at 31 at.% (in the radial direction): (a) Ga, (b) N interfacial, (c) Ga and (d) N bulk, (e) O and (f) Zn interfacial, (g) O and (h) Zn bulk atoms. The Fermi level is at 0 eV.

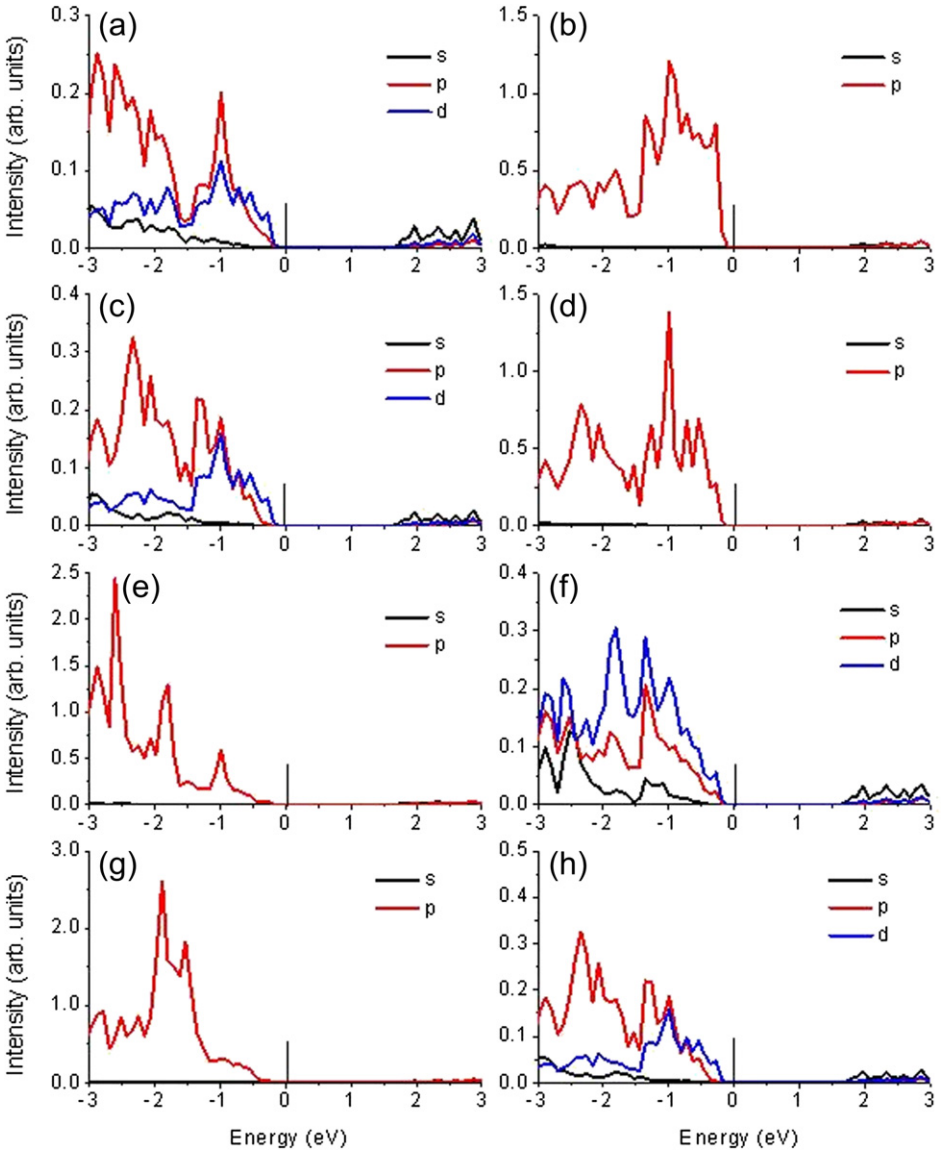

Fig. 8. The calculated partial density of states (PDOSs) of ZnO-codoped armchair GaN nanotube with concentration at 50 at.% (in the radial direction): (a) Ga, (b) N interfacial, (c) Ga and (d) N bulk, (e) O and (f) Zn interfacial, (g) O and (h) Zn bulk atoms. The Fermi level is at 0 eV.

dominated by p electrons from N atoms at the interface (low ZnO concentration), in the bulk (medium ZnO concentration), and at the interface (high ZnO concentration).

The situation is distinctive for the zigzag GaN nanotube. The band gap of the codoped nanotube decreases almost linearly with the increase of the ZnO concentration along the radial direction (Fig. 9(a)). The band gap reduces to ~1.78 eV when the ZnO hexagons are continuous in the radial direction of the nanotube and reach the concentration of 33 at.%. When the codoping is in the *z* direction, the band gap initially decreases linearly and then levels

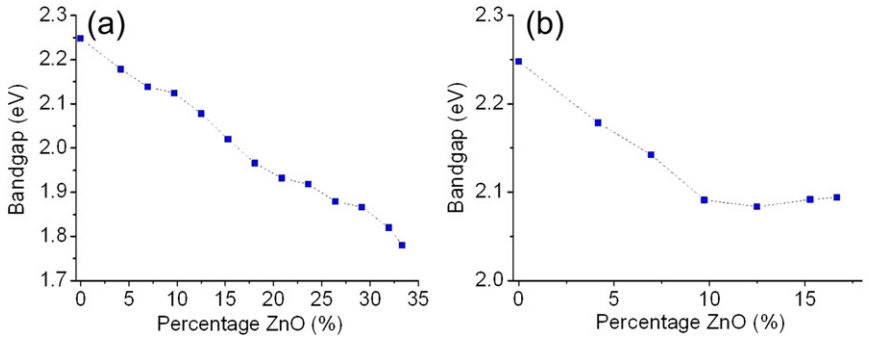

Fig. 9. The calculated band gap of zigzag (12, 0) nanotube as a function of ZnO concentration: (a) ZnO oriented in the radial direction, and (b) ZnO oriented in the *z* direction.

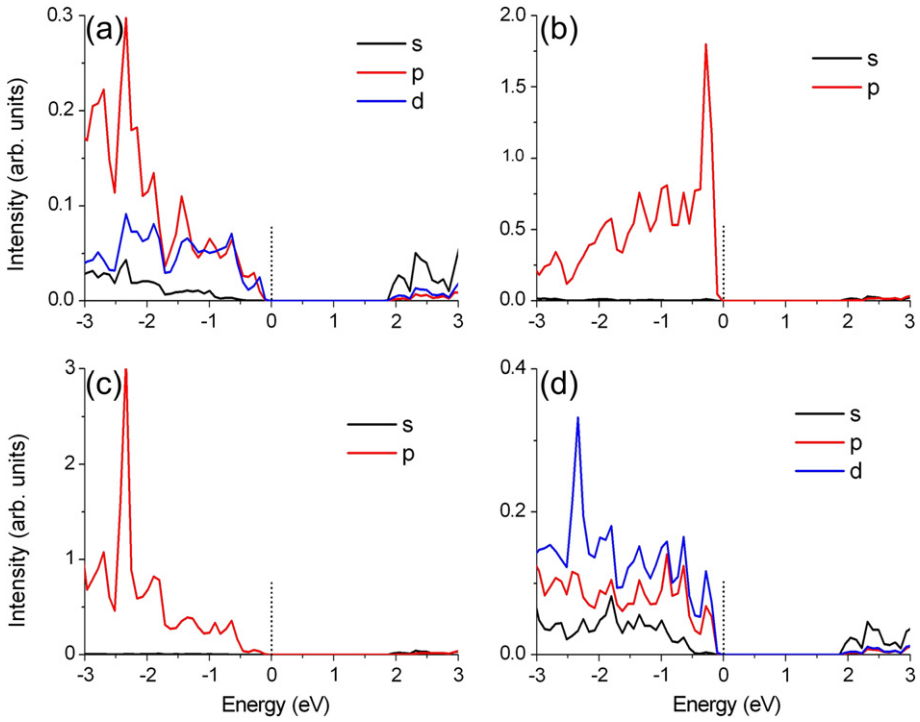

Fig. 10. The calculated partial density of states (PDOSs) of ZnO-codoped zigzag GaN nanotube with concentration at ~4.2 at.% (one hexagon ZnO): (a) Ga, (b) N, (c) O and (d) Zn interfacial atoms. The Fermi level is at 0 eV.

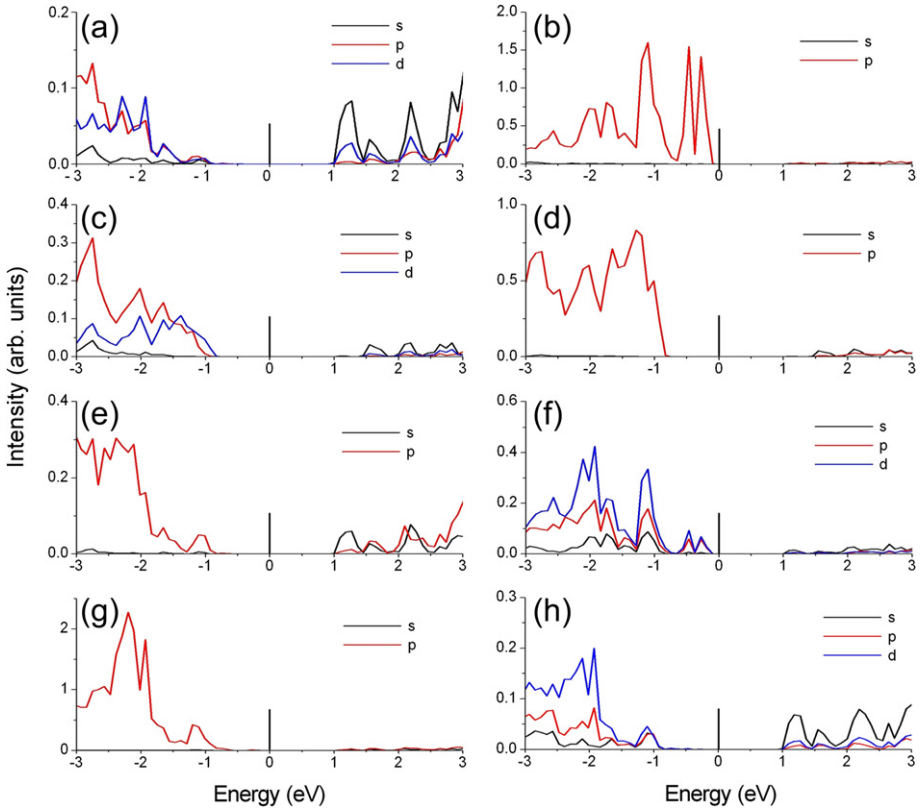

Fig. 11. The calculated partial density of states (PDOSs) of ZnO-codoped zigzag GaN nanotube with concentration at ~15.3 at.% (in the radial direction): (a) Ga, (b) N interfacial, (c) Ga and (d) N bulk, (e) O and (f) Zn interfacial, (g) O and (h) Zn bulk atoms. The Fermi level is at 0 eV.

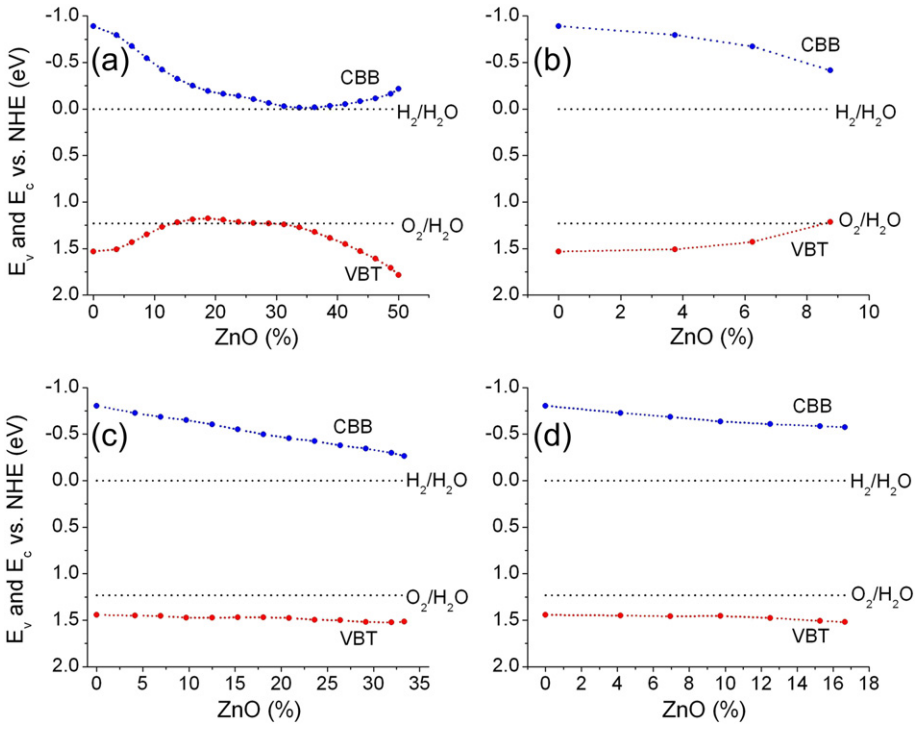

Fig. 12. The calculated CBB and VBT potentials of ZnO-codoped GaN nanotubes vs. normal hydrogen electrode (NHE) as functions of doping concentration. GaN-ac10 with codoping in (a) the radial direction and (b) the *z* direction, and GaN-zz12 with codoping in (c) the radial direction and (d) the *z* direction.

off at 2.09 eV when the concentration of the codoped ZnO hexagons is beyond 9 at.% (Fig. 9(b)). The calculated PDOSs of the codoped GaN-zz12 with the ZnO-concentration at ~4.2 at.% (one hexagon ZnO) show that that the VBT is dominated by the p electrons of N atoms (Fig. 10(b)), and the CBB is mainly attributed to s states from all of the atoms (Fig. 10). With increasing the doping concentration, the VBT (at about −1.0 eV) is still dominated by the p electrons of N interfacial atoms (Fig. 11(b)). However, the p electrons of N bulk and d electrons of Zn interfacial atoms (Fig. 11(b), (d), &(e)) are also partially contributed to the VBT. The CBB is dominantly attributed to s states from all of the interfacial atoms (Fig. 11(a), (b), (e), &(f)). The two additional levels (at about −0.46 and −0.28 eV) in PDOSs of N and Zn interfacial atoms are defect states due to the doping (Fig. 11(b) and (f)). By comparing the Figs. 5 and 6, we find that effects of the codoping on the electronic structures of GaN nanotubes are chirality-dependent. It is shown that the band structures of armchair GaN nanotubes are more easily adjusted by ZnO codoping to satisfy the requirements of optimal sunlight absorption because their band gaps can be tuned from 2.42 to 0.29 eV with the change of the ZnO concentration.

The ZnO-codoped GaN nanotubes can efficiently absorb the visible light because of their tunable band gap with the doping concentration. Besides the efficient visible-light absorption, suitable redox potentials are also prerequisites for a photocatalyst with high-efficiency for hydrogen production. The redox ability can be evaluated by aligning the VBT and CBB with respect to the water oxidation/reduction potential level. The band edges' alignment to the normal hydrogen electrode (NHE) can be obtained by [40]

$$E_{CBB} = \chi - E_e - \frac{1}{2}E_g \quad (2)$$

$$E_{VBT} = E_{CBB} + E_g \quad (3)$$

where $\chi$is the Mulliken electronegativity of the compound semiconductor, E_e is the energy of free electrons on the hydrogen scale (4.5 eV), and E_g is the calculated band gap. The Mullikan electronegativity of a compound is the geometric mean of the electronegativities of the constituent atoms [41–43]. The calculated CBBs of GaN nanotubes (both armchair and zigzag) with all of the considered ZnO-codoping concentrations are negative vs. the H_2/H_2O level (HNE) (Fig. 12), indicating that the ZnO-codoped nanotubes can reduce H^+ for H_2 production from water. Even for GaN-ac10 with the ZnO concentration at ~31 at.% in the radial direction (its band gap is about 1.27 eV), its CBB is still negative vs. NHE by −0.02 eV (its VBT is more positive than the O_2/H_2O level by 0.01 eV). Most of the codoped nanotubes show strong positive potentials, i.e. their VBTs are more positive than the O_2/H_2O level (Fig. 12), for O_2 production from water oxidization, except the GaN-ac10 with the ZnO-codoping concentration from 13 to 29 at.% in the radial direction (Fig. 12(a)) and beyond 8 at.% in the *z* direction (Fig. 12(b)). Their VBTs, however, are less positive than the O_2/H_2O level by 0.05 eV at most. Considering that the DFT method always underestimates the band gap, the experimental results of the VBTs should be more positive than the O_2/H_2O level. The production H_2 and O_2 from water under visible-light observed in GaN/ZnO alloy should be contributed to its negative CBB and strong positive VBT [27].

4. Conclusions

In summary, ZnO-codoped GaN nanotubes are designed and studied based on the first-principles calculations for their application in solar energy conversion. Our calculations reveal that the nanotubes can efficiently utilize sunlight because their band gaps can be controlled in a wide range by the codoping. It is found that the codoping and its effects on the electronic properties of the nanotubes are chirality-dependent. The codoping is easy along the radial direction for armchair nanotubes, but in the *z* direction for zigzag nanotubes because the armchair GaN–ZnO interface is more stable. The band gap can be as low as 0.29 eV for the codoped

armchair nanotube and 1.78 eV for the codoped zigzag nanotube by varying the co-dopant concentration and doping direction. The calculated band edges' potentials, CBBs and VBTs, are more negative and positive than H_2/H_2O and O_2/H_2O levels, respectively, in most the considered cases. The GaN nanotubes codoped with ZnO would be realized by various growth technologies, such as chemical vapor deposition (CVD) [44,45] and template method [46,47], with artificially controlled growth conditions. It is expected that these ZnO codoped GaN nanotubes, with a large tunable band gap, high carrier mobility, better band edges' alignments vs. the normal hydrogen electrode, and a large sunlight contact area, may find important applications in solar energy harvesting.

Acknowledgments

The DFT calculations were performed at Computational Resource Center (A*CRC) of the Agency for Science, Technology and Research (A*STAR) in Singapore.

References

[1] A. Fujishima, K. Honda, Nature 238 (1972) 37.
[2] P. Szymanski, M.A. El-Sayed, Theor. Chem. Acc. 131 (2012) 1202.
[3] E.Y. Kim, J.H. Park, G.Y. Han, J. Power Sources 184 (2008) 284–287.
[4] R. Asahi, T. Morikawa, T. Ohwaki, K. Aoki, Y. Taga, Science 293 (2001) 269–271.
[5] J.G. Yu, L.F. Qi, M. Jaroniec, J. Phys. Chem. C 114 (2010) 13118–13125.
[6] A. Trenczek-Zajac, M. Radecka, M. Jasinski, K.A. Michalow, M. Rekas, E. Kusior, K. Zakrzewska, A. Heel, T. Graule, K. Kowalski, J. Power Sources 194 (2009) 104–111.
[7] H. Pan, B.H. Gu, Z.Y. Zhang, J. Chem. Theory Comput. 5 (2009) 3074–3078.
[8] Y. Sun, G.X. Wang, K.P. Yan, Int. J. Hydrogen Energy 36 (2011) 15502–15508.
[9] S. Wendt, P.T. Sprunger, E. Lira, G.K.H. Madsen, Z.S. Li, J.O. Hansen, J. Matthiesen, A. Blekinge-Rasmussen, E. Laegsgaard, B. Hammer, F. Besenbacher, Science 320 (2008) 1755–1759.
[10] N. Rungjaroentawon, S. Onsuratoom, S. Chavadej, Int. J. Hydrogen Energy 37 (2012) 11061–11071.
[11] H. Pan, X.F. Qiu, I.N. Ivanovc, H.M. Meyer, W. Wang, W.G. Zhu, M.P. Paranthaman, Z.Y. Zhang, G. Eres, B.H. Gu, Appl. Catal. B 93 (2009) 90–95.
[12] P. Chowdhury, H. Gomaa, A.K. Ray, Int. J. Hydrogen Energy 36 (2011) 13442–13451.
[13] X.B. Chen, S.H. Shen, L.J. Guo, S.S. Mao, Chem. Rev. 110 (2010) 6503–6570.
[14] R. Dholam, N. Patel, A. Santini, A. Miotello, Int. J. Hydrogen Energy 35 (2010) 9581–9590.
[15] T. Sreethawong, C. Junbua, S. Chavadeja, J. Power Sources 190 (2009) 513–524.
[16] H. Pan, Y.W. Zhang, V.B. Shenoy, H.J. Gao, J. Phys. Chem. C 115 (2011) 12224–12231.
[17] G. Ai, W.T. Sun, X.F. Gao, Y.L. Zhang, L.M. Peng, J. Mater. Chem. 21 (2011) 8749–8755.
[18] H.H. Yang, J.J. Guo, W. Yan, H.T. Liu, J. Power Sources 156 (2006) 1305–1309.
[19] K.S. Raja, V.K. Mahajan, Misra, J. Power Sources 159 (2006) 1258–1265.
[20] X. Chen, S.S. Mao, Chem. Rev. 107 (2007) 2891–2959.
[21] M. Gratzel, Nature 414 (2001) 338–344.
[22] T. Bak, M.K. Nowotny, L.R. Sheppard, J. Nowotny, J. Phys. Chem. C 112 (2008) 12981–12987.
[23] A.L. Linsebigler, G.Q. Lu, J.T. Yates, Chem. Rev. 95 (1995) 735–758.
[24] F.E. Osterloh, Chem. Mater. 20 (2008) 35–54.
[25] X.C. Wang, K. Maeda, A. Thomas, K. Takanabe, G. Xin, J.M. Carlsson, K. Domen, M. Antonietti, Nat. Mater. 8 (2009) 76–80.
[26] H. Pan, Y.W. Zhang, V.B. Shenoy, H.J. Gao, ACS Catal. 1 (2011) 99–104.
[27] K. Maeda, K. Teramura, D.L. Lu, T. Takata, N. Saito, Y. Inoue, K. Domen, Nature 440 (2006) 295.
[28] H. Pan, B.H. Gu, G. Eres, Z.Y. Zhang, J. Chem. Phys. 132 (2010) 104501.
[29] H. Pan, Y.W. Zhang, Nano Energy 1 (2012) 488–493.
[30] P.T. Chen, C.L. Sun, M. Hayashi, J. Phys. Chem. C 114 (2010) 18228–18232.
[31] O.Z. Tan, K.H. Tsai, M.C.H. Wu, J.L. Kuo, J. Phys. Chem. C 115 (2011) 22444–22450.
[32] J.Z. Zhang, MRS Bull. 36 (2011) 48–55.
[33] P. Hohenberg, W. Kohn, Phys. Rev. B 136 (1964) B864–B871.
[34] J.P. Perdew, Y. Wang, Phys. Rev. B 45 (1992) 13244–13249.
[35] G. Kresse, J. Furthmuller, Phys. Rev. B 54 (1996) 11169–11186.
[36] H.J. Monkhorst, J.D. Pack, Phys. Rev. B 13 (1976) 5188–5192.
[37] S.M. Lee, Y.H. Lee, Y.G. Hwang, J. Elsner, D. Porezag, T. Frauenheim, Phys. Rev. B 60 (1999) 7788–7791.
[38] S.B. Zhang, J. Phys. Condens. Matter 14 (2002) R881–R903.
[39] H. Pan, Y.W. Zhang, V. Shenoy, H.J. Gao, Appl. Phys. Lett. 96 (2010) 192510.
[40] Z.J. Ma, Z.G. Yi, J. Sun, K.C. Wu, J. Phys. Chem. C 116 (2012) 25074–25080.
[41] Y. Xu, M.A.A. Schoonen, Am. Mineral 85 (2000) 543–556.
[42] M.V. Putz, N. Russo, E. Sicilia, Theor. Chem. Acc. 114 (2005) 38–45.
[43] R.G. Parr, R.G. Pearson, J. Am. Chem. Soc. 105 (1983) 7512–7516.
[44] B.D. Liu, Y. Bando, C.C. Tang, G.Z. Shen, D. Golberg, F.F. Xu, Appl. Phys. Lett. 88 (2006) 093120.
[45] Y.G. Sun, J.Q. Hu, Z.G. Chen, Y. Bando, D. Golberg, J. Mater. Chem. 19 (2009) 7592–7605.
[46] J. Dinesh, M. Eswaramoorthy, C.N.R. Rao, J. Phys. Chem. C 111 (2007) 510–513.
[47] H. Pan, C.K. Poh, Y.P. Feng, J. Lin, Chem. Mater. 19 (2007) 6120–6125.